Development of a Channel Emulator for Evaluation of MIMO-OFDM and SC-FDMA Systems

Julian Webber, Toshihiko Nishimura, Takeo Ohgane and Yasutaka Ogawa
Graduate School of Information Science and Technology, Hokkaido University
Kita 14, Nishi 9, Kita-ku, Sapporo 060-0814, Japan
E-mail: {julian.webber, nishim, ohgane, ogawa}@m-icl.ist.hokudai.ac.jp

***Abstract*—This paper describes the hardware design of a wideband radio channel emulator for evaluating the bit error rate (BER) performances of two modern communications systems. The main system application described here is a multiple input multiple output - orthogonal frequency division multiplexing (MIMO-OFDM) system with beamforming. The performance of MIMO systems are dependent on the spatial correlation between channels and this is emulated using Cholesky factorization to compute real-time channels with a desired correlation. The emulator implements various contemporary radio channel models (e.g. Gaussian, Jakes, and Zheng). Up to sixteen independent channels are programmable for a 4×4 MIMO system. The second application is single-carrier frequency domain equalization. Single carrier frequency division multiple access (SC-FDMA) is deployed in the uplink of 3GPP long term evolution (LTE) systems and uses a single-input single-output (SISO) channel. The system development on a field programmable gate array (FPGA) is described.**

I. Introduction

The performance of a communications system is highly dependent on the particular radio channel it operates within (e.g. indoor, urban or rural). A practical channel emulator should therefore be able to model a wide range of channel statistics and scenarios. With the advent of MIMO communications systems the complexity requirement for a 4×4 system has increased by at least an order of magnitude compared to that for a SISO system. Hence the design of each sub-system should ideally be of minimum complexity to enable a single-chip solution.

The layout of this paper is as follows. We first describe the channel emulator design in Section II and its hardware implementation in Section III. In Section IV a MIMO-OFDM testbed application using the emulator is detailed. In Section V we describe the second application namely frequency domain equalization (FDE). The performance results are discussed and a conclusion is drawn in Sections VI and VII respectively.

II. Channel Emulator

Three channel models were selected for implementation based on their relatively low implementation complexity. These models are: a) Gaussian independent identically distributed (IID), b) modified Jakes [1], and c) Zheng models. The Gaussian IID channel is created by summing a number of uniform random numbers in a process that is described further in Section III. The modified Jakes fading waveform, h_j, for ray-k at time-t is expressed as

$$h_J(t,k) = \sqrt{\frac{2}{N_0}} \sum_{n=1}^{N} C_{kn}\{[\cos(\beta_n)+j\sin(\beta_n)]\cos(\omega_n t+\theta_n)\} \quad (1)$$

where, N is the number of oscillators, C_{kn} is an orthogonal Walsh-Hadamard code bit, β_n is a constant phase offset, ω_n is the Doppler shift and θ_n is an initial phase.

The fading on the real branch of the Zheng model is expressed as

$$h_Z(t,k) = \sqrt{\frac{2}{N}} \sum_{n=1}^{N} \{\cos(2\pi f_D T_s m \cos(\alpha_n[m] + \phi_n)\} \quad (2)$$

where, f_D is the maximum Doppler frequency, $\alpha_n = 2\pi n - \pi + \theta[n]/4N$. The initial phase ϕ_n and θ are both initialized with a different uniform random angle distributed on $[-\pi, \pi)$ [2].

Two important parameters affecting the performance of a MIMO system are the ratio of direct to indirect paths expressed by the Rician K-factor and also the correlation between sub-channels [3]. As the correlation between MIMO sub-channels increases, the system performance degrades. To apply a specific level of correlation with low complexity we first construct the MIMO channel covariance matrix $\boldsymbol{C}$ from the Kronecker product of the mobile transmitter $\boldsymbol{R}_{\text{MS}}$ and receiver $\boldsymbol{R}_{\text{BS}}$ correlation matrices [4]. The Cholesky factorization of $\boldsymbol{C} = \boldsymbol{L}\boldsymbol{L}^T$, is then provided by the lower diagonal matrix $\boldsymbol{L}$. The vector of correlated samples $\boldsymbol{Z}$, is then obtained by multiplying $\boldsymbol{L}$ with an input vector of Gaussian samples $\boldsymbol{V}$, as shown by

$$\begin{pmatrix} Z_1 \\ Z_2 \\ Z_3 \\ \vdots \\ Z_m \end{pmatrix} = \begin{pmatrix} 1 & 0 & 0 & \cdots & 0 \\ l_{21} & l_{22} & 0 & \cdots & 0 \\ l_{31} & l_{32} & l_{33} & \ddots & \vdots \\ \vdots & \vdots & \vdots & \ddots & 0 \\ l_{m1} & l_{m2} & l_{m3} & \cdots & l_{mm} \end{pmatrix} \begin{pmatrix} V_1 \\ V_2 \\ V_3 \\ \vdots \\ V_m \end{pmatrix}. \quad (3)$$

A single line-of-sight ray may be dominant while the remaining scattered rays sum to form a Rayleigh distribution. The fading signal is represented as

$$y(n) = \sqrt{\frac{K}{1+K}} x_d(n) + \sqrt{\frac{1}{1+K}} x_i(n), \quad (4)$$

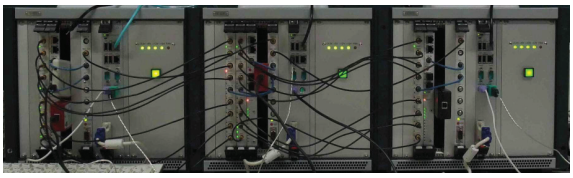

Fig. 1. Channel emulator (centre) together with TX and RX systems.

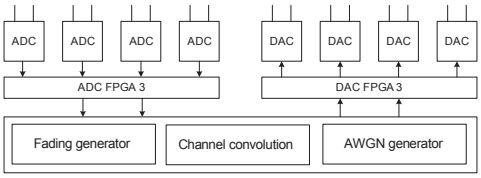

Fig. 2. Channel emulator block diagram.

where $x_d(n)$ and $x_i(n)$ are the dominant and indirect paths respectively at sample n. When K is zero the channel suffers deep fades and as K approaches infinity the direct component becomes dominant.

III. Hardware Implementation

The channel emulator is implemented on a base Koden E-1071 processing platform [5]. The main signal processing card contains four Analog Devices TigerSharc TS-201 DSPs and three Xilinx Virtex-4 FPGAs. The correlated MIMO channels are created on the LX100 FPGA on the DSP card. Up to four complex baseband MIMO TX/RX signals are routed via SMA connectors to 8 DACs/ADCs on the signal conditioning cards. Two additional E-1071 base units are deployed for the TX and RX and programmed either with the MIMO-OFDM or SC-FDE software code (Fig. 1). A block diagram of the channel emulator is shown in Fig. 2.

The waveform representing each scattered signal is modeled as a sinusoid and generated from a 16-bit sine and cosine look-up table (LUT). A counter with step-size proportional to the Doppler frequency is used as the LUT address generators. Upto sixteen scattered signals are then summed with care taken to avoid a summation overflow. By using a 20-bit adder an overflow does not occur even if all signals have a maximum value. The source code was written directly in VHDL language with Q-format arithmetic used throughout the design [6]. A benefit of this method is the control over every module implementation. However, for large designs the development and testing times are particularly increased when compared with a library-block approach such as [7].

The multipath delays are implemented using a tapped delay line, and specific tap delays can be set at run-time with the Xilinx programmable shift register [8]. Each register has a maximum size of sixteen samples and five can be cascaded together to provide delays up to 800 ns. The average power gain on each tap can be set either at run-time or according to a desired channel profile. The sampled ADC signal on the nth receive branch is then convolved with the mth TX channel $h_{nm}(t)$, using a finite impulse response filter (FIR).

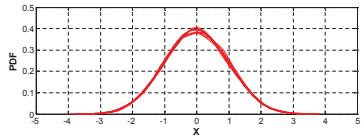

Fig. 3. Gaussian PDF distribution.

Each uniform random variable (URV) was generated from the output of a feedback shift register with the feedback taps tabulated in [8]. A feedback delay-line requires very few resources and so relatively long registers were used (20-50 bits) to ensure each uniform and hence also Gaussian signals were completely independent and had repeat times far longer than a typical session. For each channel n an independent URV is created for β_n and θ_n. A Gaussian sample was created by summing twelve URV. This produces a sample with a variance of one and is an eleventh-order polynomial approximation to the normal distribution [9] with samples in the range $\pm 6\sigma$. Each fading generator used a different combination of seed, seed-offset and M-sequence length. The four complex AWGN PDF distributions are shown in Fig. 3. An improved generator based on the Box-Muller method is also being designed which improves accuracy by placing more samples in the non-linear (tail) sections of a logarithmic function.

The complexity of the time domain emulator is approximately proportional to $N_T \times N_R \times M$, where N_T and N_R are the number of transmitters and receivers respectively and M is the number of resolvable paths. The ADCs and DACs have 16-bit resolution allowing a high dynamic range to be achieved. Xilinx 18-bit multipliers have been used to facilitate the fixed-point design though it is reported that fewer bits can be used with a small reduction in performance [10].

IV. MIMO-OFDM with Eigenbeamforming

The MIMO channel capacity is optimized when the transmitter directs orthogonal beams through a transmit weight matrix $\boldsymbol{W}_{\mathrm{TX}}$ on each substream [11]. This technique is termed eigenbeam-space division multiplexing (E-SDM). The signals are detected by a receive weight matrix $\boldsymbol{W}_{\mathrm{RX}}$ at the receiver. The optimal weights are given by eqns (5, 6)

$$\boldsymbol{W}_{\mathrm{Tx}} = \boldsymbol{U}\sqrt{\boldsymbol{P}}, \tag{5}$$

$$\boldsymbol{W}_{\mathrm{Rx}} = \boldsymbol{U}^H \boldsymbol{H}^H, \tag{6}$$

where $\boldsymbol{P} = \mathrm{diag}(P_1, \cdots, P_K)$ is the transmit power matrix, $\boldsymbol{H}^H$ is the Hermitian transpose of the channel in the frequency domain $\boldsymbol{H}$ and $\boldsymbol{U} \in \mathbb{C}^{N_{\mathrm{T}} \times K}$ is obtained from the eigenvalue decomposition (EVD) as (7):

$$\boldsymbol{H}^H \boldsymbol{H} = \boldsymbol{U}\boldsymbol{\Lambda}\boldsymbol{U}^H, \tag{7}$$

$$\boldsymbol{\Lambda} = \mathrm{diag}(\lambda_1, \cdots, \lambda_K). \tag{8}$$

where, Λ is a matrix of eigenvalues of $\boldsymbol{H}^H\boldsymbol{H}$, and the columns of $\boldsymbol{U}$ are the corresponding eigenvectors.

The principle blocks of the MIMO-OFDM system [12] are shown in Fig. 4. At the transmitter, the input data is scrambled and channel encoded using forward error correction

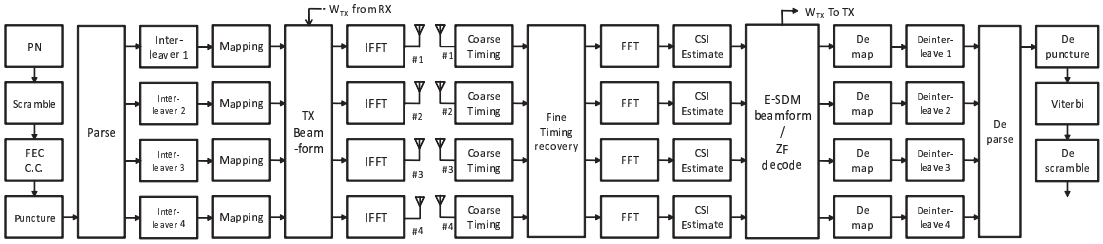

Fig. 4. MIMO-OFDM beamforming transceiver block diagram.

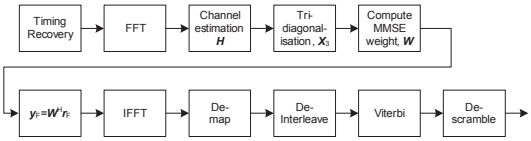

Fig. 5. SC-FDE receiver block diagram.

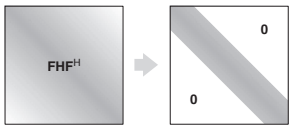

Fig. 6. Channel tri-diagonalization concept.

(FEC). The interleaver distributes bits across non-consecutive subcarriers. After puncturing and symbol mapping, a 64-point IFFT converts the data from the frequency to time domains. Two stages are required in the transmission of one data packet. First, a non-beamformed sounding packet is sent enabling the RX to estimate the MIMO channel. The actual beamforming is applied in the next packet. A Modelsim testbench was written to test each block of the FPGA code by comparing the results with a Matlab model.

V. SC-FDE

Single carrier systems exhibit a lower peak to average power ratio (PAPR) compared to OFDM systems, which require a larger and more inefficient power amplifier back-off. Further, the complexity burden of the single carrier system is shifted from the mobile transmitter to the base-station receiver [13]. The SC-FDE receiver block diagram (Fig. 5) shares many functional blocks with that of an OFDM system [14]. The IFFT function that was in the MIMO-OFDM transmitter is moved to the receiver side. In a fast fading channel, however, the reduction of intersymbol interference is required and frequency domain equalization is a low complexity method to achieve this. At the transmitter a cyclic prefix (CP) is appended to an FDE data block, $\boldsymbol{s}$. The received signal vector after CP removal is then given by

$$\boldsymbol{r} = \boldsymbol{H}\boldsymbol{s} + \boldsymbol{n}, \tag{9}$$

where $\boldsymbol{H}$ is the $N \times N$ channel matrix and $\boldsymbol{n}$ is Gaussian noise. After computing an $N \times N$ DFT at the RX, we have

$$\boldsymbol{F}\boldsymbol{r} = \boldsymbol{F}\boldsymbol{H}\boldsymbol{s} + \boldsymbol{F}\boldsymbol{n} \tag{10}$$

$$= \boldsymbol{F}\boldsymbol{H}\boldsymbol{F}^H\boldsymbol{F}\boldsymbol{s} + \boldsymbol{F}\boldsymbol{n}. \tag{11}$$

If the channel is static within a block, $\boldsymbol{H}$ is a cyclic matrix and can be diagonalized by $\boldsymbol{F}$ as $\boldsymbol{F}\boldsymbol{H}\boldsymbol{F}^H = \boldsymbol{D} = \mathrm{diag}(d_1, \ldots, d_N)$. Therefore, (11) can be written as

$$\boldsymbol{r}_F = \boldsymbol{D}\boldsymbol{s}_F + \boldsymbol{n}_F, \tag{12}$$

where $\boldsymbol{r}_F = \boldsymbol{F}\boldsymbol{r}$, $\boldsymbol{s}_F = \boldsymbol{F}\boldsymbol{s}$, and $\boldsymbol{n}_F = \boldsymbol{F}\boldsymbol{n}$ are the frequency domain received, transmitted, and noise vectors respectively.

The equalized signal is obtained by multiplying the received vector with the Hermitian transpose of a weight matrix $\boldsymbol{W}$ as

$$\boldsymbol{y}_F = \boldsymbol{W}^H\boldsymbol{r}_F, \tag{13}$$

where $\boldsymbol{W}$ is the optimum weight in the minimum mean square error (MMSE) sense and is given by

$$\boldsymbol{W} = (\boldsymbol{D}\boldsymbol{D}^H + \sigma^2\boldsymbol{I})^{-1}\boldsymbol{D}, \tag{14}$$

where σ^2 denotes the frequency domain noise power. It can be seen that the computation of the weight matrix has low complexity ($\mathcal{O}(N)$) as $\boldsymbol{D}\boldsymbol{D}^H + \sigma^2\boldsymbol{I}$ is a diagonal matrix.

The transmitted signal is then estimated by computing the IFFT of the FDE output. i.e. $\boldsymbol{y} = \boldsymbol{F}^H\boldsymbol{y}_F$. If the channel changes within an FDE time slot then the channel cyclicity is lost, i.e., $h_l(0) \neq \cdots \neq h_l(N-1)$ for all l. In this case, $\boldsymbol{F}\boldsymbol{H}\boldsymbol{F}^H$ becomes a square matrix $\boldsymbol{X}$ and is no longer diagonal. Through an analysis of the relationship between $\boldsymbol{X}$ and the channel variation quantity, it was shown in [15] that

$$X_{(p,q)} = \begin{cases} \sqrt{N}\{f_q(0) + (N-1)\Delta f_q/2\} & \text{for } p = q \\ \dfrac{-\sqrt{N}\Delta f_q}{1 - e^{-j2(p-q)\pi/N}} & \text{for } p \neq q \end{cases}, \tag{15}$$

where $X_{(p,q)}$ denotes the (p,q)th component of $\boldsymbol{X}$. Using this equation, the complexity of computing $\boldsymbol{X}$ decreases from $\mathcal{O}(N^2 \log N)$ to $\mathcal{O}(N \log N)$. The non-diagonal term in (15) is expected to diminish rapidly as $|p-q|$ increases. Therefore, $\boldsymbol{X}$ was approximated as a tri-diagonal matrix $\boldsymbol{X}_3$ by forcing $X_{(p,q)} = 0$ for $|p-q| > 1$ as shown in Fig. 6.

To enable the accurate channel estimate in the presence of multipath and multiple access interference, special cyclic prefixes called constant amplitude zero auto-correlation (CAZAC) are required [16]. The n-th value of the k-th Zadoff-Chu CAZAC sequence for odd(even) L ($e = 1(0)$) is given by

$$\boldsymbol{c}_k(n) = \exp\left[\frac{j2\pi k}{L}(n + n\frac{n+e}{2})\right], \tag{16}$$

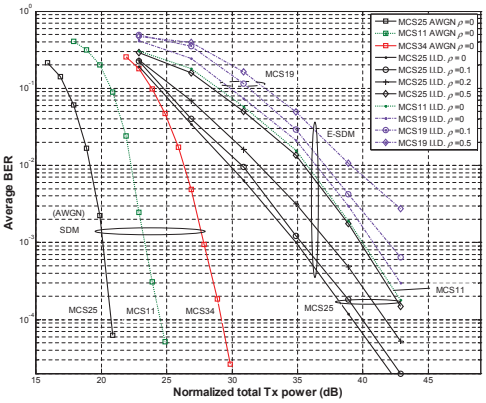

Fig. 7. BER performance of SDM in AWGN and E-SDM systems in I.I.D. channels with increasing correlation.

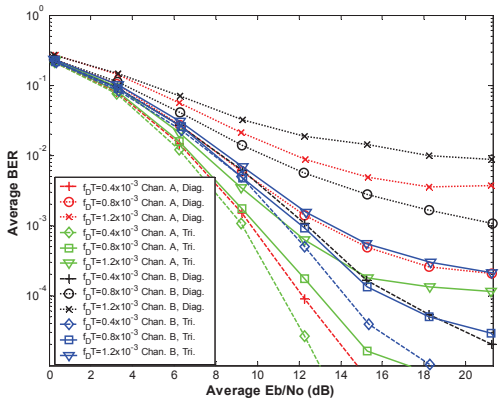

Fig. 8. BER performance of FDE with diagonalization and tridiagonalization. Chan A = {0, -1,...-15dB} and Chan B = {0,-1,-2,-3dB}.

VI. Performance Results

The MIMO-OFDM performance with and without beamforming were evaluated using ModelSim software. This simulates the exact hardware response using the VHDL code used in the final hardware compilation. The SDM results refer to those from an AWGN uncorrelated channel (Fig. 7). For E-SDM systems, a packet consisting of N_T times 40 OFDM symbols was transmitted over 64 arbitrary Gaussian 2×2, 3×3 and 4×4 single-tap MIMO channels with $\rho = 0.0$, 0.1, 0.2 and 0.5. The number of bits per substream were therefore {4,4}, {4,4,4}, {2,2,2,2}, {6,2} and correspond to IEEE 802.11n modulation coding scheme (MCS) values 11, 19, 25 and 34 respectively [17]. For the MCS25 system, an additional (0.3 dB, 2.4 dB and 5.4 dB) transmit power was required when ρ was increased from 0.0 to (0.1, 0.2. and 0.5) respectively in order to maintain a constant 10^{-3} BER.

The performance of the SC-FDE system was simulated assuming a block size of 256 samples with BPSK modulation. Two channels were modeled using the Jakes fading model: Chan A has 16 delay taps while Chan B has 4 taps with 1 dB attenuation per tap. The data was convolutionally encoded ($R_c = 0.5$). The performance results are measured as a function of the normalized Doppler frequency f_DT, where f_D is the maximum Doppler frequency and T is the symbol duration. Figure 8 shows the BER performance of the FDE compared with conventional diagonalization. At a target BER of 10^{-3} when $f_DT = 0.8 \times 10^{-3}$, the tridiagonalization performance is 3.0 dB and 8.4 dB improved with respect to that of diagonalization in Chan A and Chan B respectively. Current work is extending the hardware FDE block size from N=64 to 256 symbols and complete the DSP-FPGA interface for the feedback of computed diagonalized weights.

VII. Conclusion

The design and implementation aspects of a channel emulator for investigating the performance of modern communications systems in fading channels has been described. The implementation of three low-complexity channel models were described. The initial phase of each scattered ray was generated from the output of an M-sequence shift register. Similarly, a Gaussian noise process was created from summing several independent M-sequences. For a 4×4 MIMO-OFDM system with QPSK modulation, the performance degraded by 2.4 dB when the correlation coefficient was 0.2.

References

[1] P. Dent, G. Bottomley, and T. Croft, "Jakes fading model revisited," *Electronics Letters*, vol. 29, no. 13, pp. 1162-1163, June 1993.

[2] Y. Zheng and C. Xiao, "Simulation models with correct statistical properties for Rayleigh fading channels," *IEEE Trans. on Comms.*, vol. 51, No. 6, pp. 920–928, Jun. 2003

[3] V. Tarokh, N. Seshadri, and A. Calderbank, "Space-time codes for high data rate wireless communications Performance and codes construction," *IEEE Trans. Inform. Theory*, vol. 44, pp. 744-765, Mar. 1998.

[4] D. Shiu, G. Foschini, M. Gans, and J. Kahn, "Fading correlation and its effect on the capacity of multi-element antenna systems," *IEEE Trans. Commun.*, vol. 48, no. 3, pp. 502–513, Mar. 2000.

[5] "E-1072 signal processing platform," *Koden Electronics*, 2008.

[6] N. Dahnoun, "Digital signal processing implementation: Using the TMS320C6000 DSP platform", Prentice Hall, 2000.

[7] "System Generator for DSP," Xilinx User Guide Release 10.1, Mar. 2008.

[8] M. George and P. Alfke, "Linear feedback shift registers in Virtex devices," Xilinx Application Report XAPP210, Apr. 2007.

[9] N. L. Johnson, S. Kotz, and N. Balakrishnan, "Continuous uni-variate distributions," *John Wiley*, vol. 2, 2nd Ed., New York, 1995.

[10] K. Borries, G. Judd, D. Stancil, and P. Steenkiste, "FPGA-based channel simulator for a wireless network emulator," *Proc. IEEE VTC*, May 2009.

[11] T. Ohgane, T. Nishimura, and Y. Ogawa, "Applications of space division multiplexing and those performance in a MIMO channel," *IEICE Trans. Commun.*, vol. E88-B, no. 5, pp. 1843–1851, May 2005.

[12] Y. Cho, J. Kim, W. Yang, and C. Kang, "MIMO-OFDM wireless communications with Matlab," *Wiley*, 2010.

[13] T. Tavangaran, A. Wilzeck, and T. Kaiser, "MIMO SC-FDMA system performance for space time / frequency coding and spatial multiplexing," *IEEE WSA'08*, Darmstadt, Feb. 2008.

[14] J. Coon, J. Siew, M. Beach, A. Nix, S. Amour, and J. McGeehan, "A comparison of MIMO-OFDM and MIMO-SCFDE in WLAN environments," *Globecom'03*, San Francisco, Dec. 2003.

[15] K. Saito, J. Webber, T. Nishimura, T. Ohgane, and Y. Ogawa, "Tri-diagonalizing approach on frequency domain equalization in a doubly-selective channel," *Globecom'09*, Hawaii, Dec. 2009.

[16] Y. Wen, W. Huang, and Z. Zhang, "CAZAC sequence and its application in LTE random access," *IEEE ITW'06*, pp. 544-547, Chengdu, Oct. 2006.

[17] "IEEE P802.11 wireless LANs joint proposal: High throughput extension to the 802.11 standard: PHY," *IEEE 802.11-05/1102r4*, Jan. 2006.